PL-TR--96-2152
Environmental Research Papers, No. 1197

EARTHQUAKE FOCAL MECHANISMS IN NORTHEASTERN CHINA AND KOREA DETERMINED BY THE GRID SEARCH ALGORITHM

John J. Cipar

29 August 1996

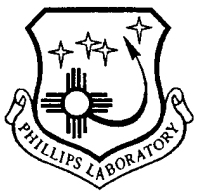

PHILLIPS LABORATORY
Directorate of Geophysics
AIR FORCE MATERIEL COMMAND
HANSCOM AIR FORCE BASE, MA 01731-3010

This technical report has been reviewed and is approved for publication.

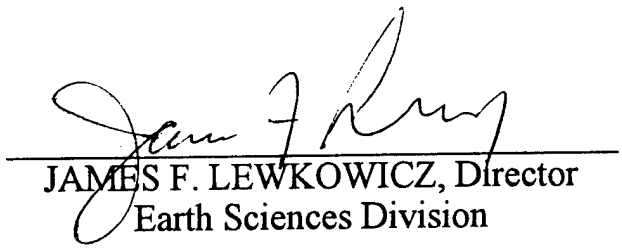

JAMES F. LEWKOWICZ, Director
Earth Sciences Division

This report has been reviewed by the ESC Public Affairs Office (PA) and is releasable to the National Technical Information Service (NTIS).

Qualified requestors may obtain additional copies from the Defense Technical Information Center (DTIC). All others should apply to the National Technical Information Service (NTIS).

If your address has changed, if you wish to be removed from the mailing list, or if the addressee is no longer employed by your organization, please notify PL/IM, 29 Randolph Road, Hanscom AFB, MA 01731-3010. This will assist us in maintaining a current mailing list.

Do not return copies of this report unless contractual obligations or notices on a specific document requires that it be returned.

REPORT DOCUMENTATION PAGE

Form Approved
OMB No. 0704-0188

1. AGENCY USE ONLY *(Leave blank)*	2. REPORT DATE	3. REPORT TYPE AND DATES COVERED
	29 August 1996	Scientific

4. TITLE AND SUBTITLE
Earthquake Focal Mechanisms in Northeastern China and Korea Determined by the Grid Search Algorithm

5. FUNDING NUMBERS
PR 2309
TA G2
WU 10

6. AUTHOR(S)
John J. Cipar

7. PERFORMING ORGANIZATION NAME(S) AND ADDRESS(ES)
Phillips Laboratory/GPE
29 Randolph Road
Hanscom AFB, MA 01731

8. PERFORMING ORGANIZATION REPORT NUMBER
PL-TR-96-2152
ERP, No. 1197

9. SPONSORING / MONITORING AGENCY NAME(S) AND ADDRESS(ES)
AFOSR/NM
Bolling AFB, DC

10. SPONSORING / MONITORING AGENCY REPORT NUMBER

11. SUPPLEMENTARY NOTES

12a. DISTRIBUTION / AVAILABILITY STATEMENT
Approved for public release; distribution unlimited

12b. DISTRIBUTION CODE

13. ABSTRACT *(Maximum 200 words)*

The grid search algorithm for determining earthquake focal mechanism and depth is tested by inverting regional-distance seismograms for a suite of five earthquakes in northeastern China and Korea. An improved crustal model for the region is used to compute the synthetic Green's functions for the eight fundamental fault types. To account for uncertainty in timing, location, and crustal structure, the synthetics are time shifted during the inversion to produce the best match. This process is repeated at a range of source depths. The focal mechanisms and depths for the earthquakes studied in this report are broadly consistent with teleseismic measurement of earlier large events in the region. The average time delays at each station and for each event provide a measure of the uncertainty in origin time and velocity structure. Either crustal velocity variations of 1-2 percent, or incorrect event locations of about 10 km, could explain the observed delays.

14. SUBJECT TERMS
Seismology, Earthquakes, Crustal Structure, China, Korea

15. NUMBER OF PAGES
32

16. PRICE CODE

17. SECURITY CLASSIFICATION OF REPORT	18. SECURITY CLASSIFICATION OF THIS PAGE	19. SECURITY CLASSIFICATION OF ABSTRACT	20. LIMITATION OF ABSTRACT
Unclassified	Unclassified	Unclassified	SAR

Contents

Illustrations

Tables

Acknowledgments

I wish to thank Delaine Reiter and Anton Dainty for critically reading the manuscript. Mary Martyak edited the final draft. The assistance of Stephan Koester and the Data Management Center of the Incorporated Institutions of Seismology in providing the data used in this report is gratefully acknowledged. This work was supported under AFOSR Task 2309G2 Seismology at Phillips Laboratory.

Earthquake Focal Mechanisms in Northeastern China and Korea Determined by the Grid Search Algorithm[1]

1. INTRODUCTION

Knowledge of the focal mechanism and depth of an earthquake is fundamental information for tectonic studies, hazard mitigation, and seismic discrimination. Early in this century, the discovery of deep earthquakes eventually led to the plate subduction hypothesis. Numerous focal mechanisms, determined in the 1960s using data from the newly installed World Wide Standardized Seismograph Network, helped gain acceptance for the sea floor spreading model of continental drift. In the field of nuclear test discrimination, event depth is considered to be crucial to discrimination, since events below 5 km are highly unlikely to be explosions. A focal mechanism with clear dilatational first-motions is a strong (although not fool proof) indicator that the source is an earthquake, rather than an explosion.

In recent years, the emphasis in nuclear test monitoring has shifted from yield measurements of large explosions to discrimination between small magnitude earthquakes and explosions under a Comprehensive Test-Ban Treaty (CTBT). Observationally, this has meant emphasis on analysis of signals recorded at regional distances, generally defined to be less than about 2000 km. The events of interest are small and often fall below earth noise at long ranges. Regional seismograms are considerably more complex and variable than those recorded at longer, or teleseismic, distances because the regional travel path is primarily in the complex, heterogeneous crust and upper mantle of the Earth.

My goal in this report is to further develop and test a grid search algorithm for determining earthquake focal mechanisms and depth (Zhao and Helmberger, 1994; Cipar, 1995). A suite of mb ~ 4.0-5.1 events from northeastern China and Korea are studied (Figure 1). These events are well recorded by a modern high dynamic range network, the Chinese Digital Seismograph Network (CDSN), which provides on-scale recordings of these moderate-size earthquakes. Furthermore, the earth structure in this region appears to be rather homogenous, at least to long-period surface waves, which allows the use of a single set of synthetic Green's functions for waveform inversion (Cipar, 1995).

Received for publication 29 August 1996

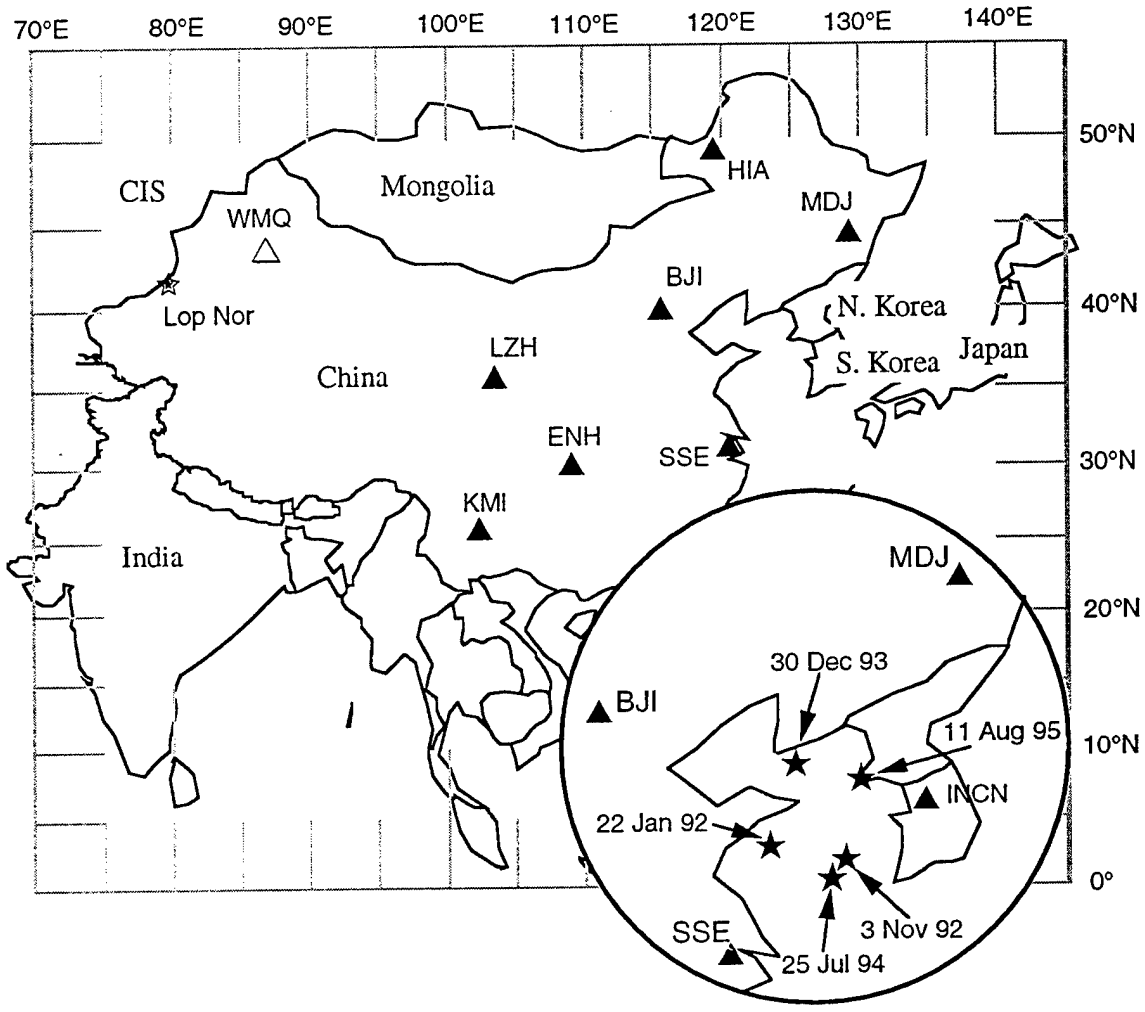

Figure 1. Map of eastern Asia showing the CDSN stations (triangles). The Chinese test site at Lop Nor is shown by an open star. The inset shows the events studied in this report (stars) and nearby CDSN stations.

Table 1. Earthquake Information

Earthquake	Origin Time h:m:s	Latitude (deg N)	Longitude (deg W)	Depth (km)	mb	Ms	Ml (BJI)	Location
22 January 1992	21h 41m 25.9s	35.351	121.109	33 N	5.1	4.8	5.5	W. Yellow Sea
3 November 1992	17h 31m 23.7s	35.328	123.312	10	4.8	-	5.0	Yellow Sea
30 December 1993	16h 29m 49.8s	38.257	122.656	33 N	4.6	-	4.8	NE China
25 July 1994	17h 41m 50.6s	35.015	124.447	10 G	5.0	5.0	-	Yellow Sea
11 August 1995	18h 17m 44.4s	38.029	124.441	10 G	4.0	-	3.8	N Korea

Focal mechanisms and depths of these recent, moderate-size earthquakes will be compared to larger events in the region that have been studied using teleseismic data.

2. DATA AND ANALYSIS TECHNIQUE

Northeastern China, while not as seismically active as the adjacent Japanese arc, is a region of moderate seismicity that has experienced a number of large, damaging earthquakes throughout history (Cipar, 1979; Chung and Cipar, 1983; Chung and Brantley, 1989). For this report, I selected recent earthquakes that occurred in and around the Korean peninsula for analysis (Table 1). An important criterion was that the events were recorded by the Chinese Digital Seismographic Network (Table 2). This network provides excellent on-scale recordings of moderate-size earthquakes at regional distances. Five events that had adequate signal-to-noise ratio at a minimum of two stations (Table 1) were selected from the waveform database maintained by the Incorporated Research Institutions for Seismology (IRIS). The largest event was the 25 July 1994 Yellow Sea earthquake (Ms = 5.0) for which the US Geological Survey (USGS) centroid moment tensor solution has been determined. The other four events were too small to allow a reliable long-period moment tensor solution. Of particular interest in the context of CTBT monitoring is the mb = 4.0 event that occurred in North Korea, a country of US monitoring concern. The event is too small to be clearly observed at teleseismic

Table 2. CDSN Station Information

Station	Latitude (°N)	Longitude (°E)	Elevation (m)	Location
BJI	40.0403	116.1750	43.0	Beijing
ENH	30.2800	109.4975	487.0	Enshi
HIA	49.2667	119.7417	610.0	Hailar
HKC	22.3036	114.1719	0.0	Hong Kong
INCN	37.4833	126.6333	410.0	Inchon, South Korea
KMI	25.1500	102.7500	1952.0	Kunming
LZH	36.0867	103.8444	1560.0	Lanzhou
MDJ	44.6164	129.5919	250.0	Mudanjiang
SSE	31.0956	121.1867	10.0	Sheshan

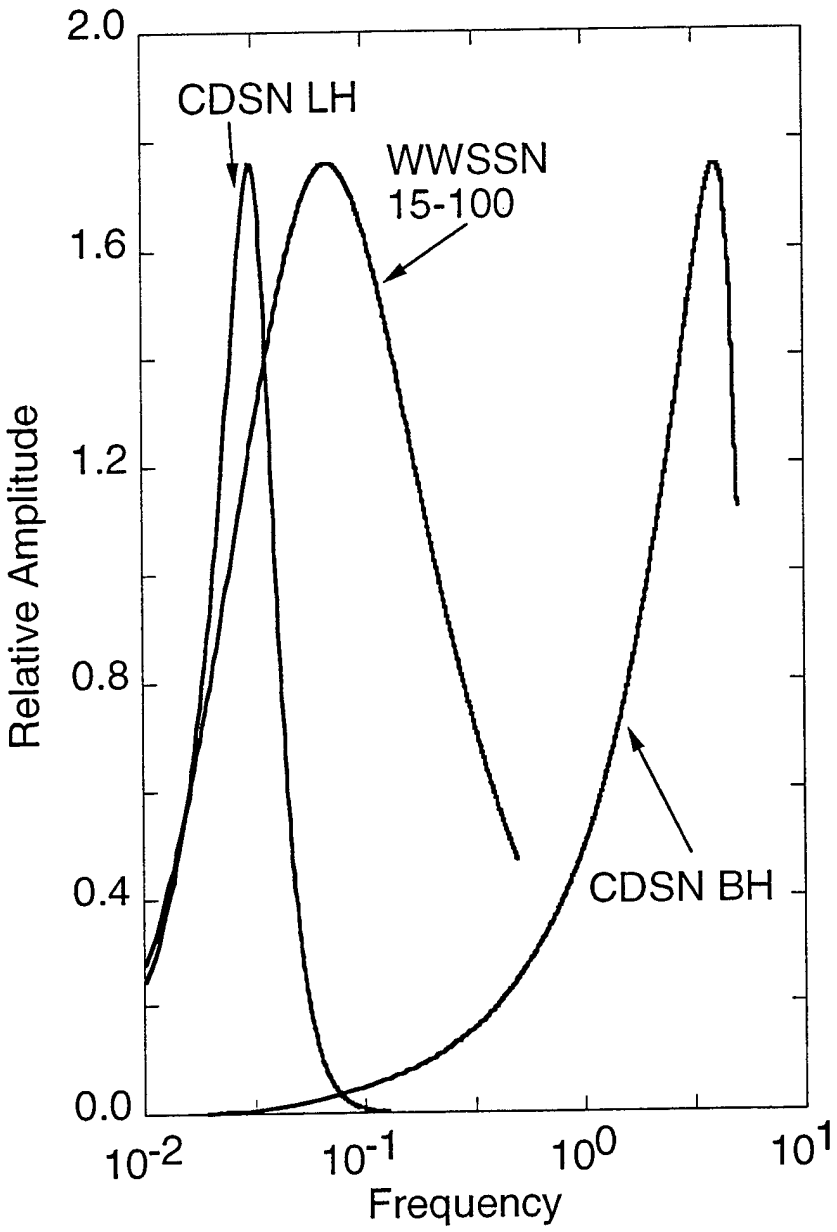

Figure 2. Instrument amplitude response as a function of frequency for three common seismograph systems.

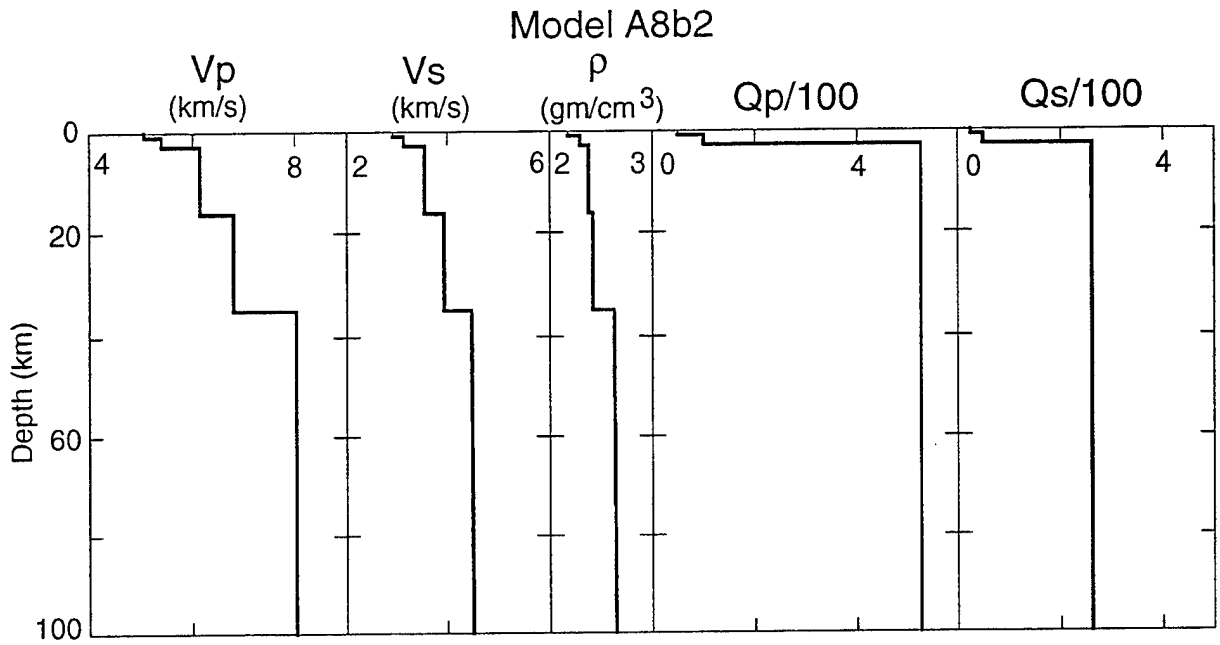

Figure 3. Parameters of Model A8b2 displayed as a function of depth. (see Table 3).

distances, thus regional observations are crucial to determining source parameters.

Both long-period (LH) and broad-band (BH) seismograms were obtained from IRIS. The LH band data are used in the focal mechanism inversions, and first-motion observations were made from the BH records. For each event, the data were first detrended and windowed to isolate the surface wave signal, and then high-pass filtered with a three-pole Butterworth filter with a corner frequency of 0.01 Hz. I prefer to work with data that have suffered as little processing as possible. In particular, I use observed data that still retain the instrument response, and compare these directly to synthetics that have been convolved with the appropriate instrument response. The instrument response acts like a causal filter, producing seismograms that are similar to familiar analog records. To equalize the data to a common response, I first deconvolve out the original response, then convolve in the response of a specific station, in this case the LHZ component at the CDSN station MDJ (Figure 2). This procedure is done in one pass in the frequency domain, and works especially well for stations with similar instrument response functions, such as most of the CDSN stations, in which the only effect is a scale change. The CDSN stations are currently being upgraded to full compatibility with other IRIS stations with a major change in instrumentation. Station HIA was upgraded before the 11 August 1995 North Korean earthquake. In addition, the IRIS station INCN (Inchon, South Korea) was operating for that event. The IRIS response is given in units of velocity, unlike the CDSN, which is in units of displacement. The velocity response is much broader band than the original CDSN. For these stations, I deconvolved out the velocity response, integrated, and convolved in the CDSN response. The observed and synthetic seismograms shown in this report are in units of counts that can be scaled to units of meters at 0.04 Hz by dividing by the sensitivity of 1.97×10^9 counts/meter. The synthetics were computed as displacement seismograms and convolved with the CDSN instrument response for the LHZ component at station MDJ. The instrument-corrected horizontal seismograms were rotated to radial and transverse components. In this way, observed and synthetic seismograms are directly comparable to each other in the time domain.

The grid search method has been discussed in Zhao and Helmberger (1994) and Cipar (1995); specifics of the algorithm used in this report are given in Cipar (1995). Synthetic seismograms are constructed from a set of eight fundamental fault Green's functions computed at a range of distances and depths using reflectivity (Fuchs and Muller, 1971; Muller, 1985). The program selects the set of Green's functions closest in distance to each station and weights these according to the focal mechanism to produce the synthetic. This is done for a grid of strike, dip, and rake values over the entire focal

sphere for a given source depth. Synthetic and observed seismograms are compared using the L2 norm (Menke, 1984). The procedure is repeated for a range of source depths. The focal mechanism/depth combination with the lowest L2 norm provides the best agreement between observed and synthetic seismograms. A further constraint is P-wave polarity readings. The program rejects trial mechanisms that do not fit the observed P-wave polarity readings. The program has a feature that allows trial mechanisms that have a user-specified number of incorrect readings. This feature is useful in the case of unclear readings, or readings near a nodal line. Another feature of the algorithm allows the synthetics to be shifted in time relative to the observed data, accounting for uncertainties in the event origin time and differences in the group velocity for each source-to-station path.

I assume that each of the events studied in this report is an earthquake, based upon the observation of clear, strong Love waves on the transverse component. For this reason, the data were not tested against explosion synthetics. An explosion source in a one-dimensional earth model (such as A8b2) produces no transverse component. A future improvement to the algorithm will allow non-double couple source mechanisms, such as explosions.

3. SEISMIC MODEL

The Green's functions used in the inversions in this report were computed with a improved version of the A8 model for northeastern China and the Yellow Sea (Cipar, 1995). The current model is A8b2, which has a thinner crust (35-km versus 40-km for A8), higher Pn velocity (8.04 km/sec), and higher velocities in the sediments than A8 (Table 3 and Figure 3). In addition, A8b2 uses the IASPEI91 upper mantle velocities (Kennett, 1991). Synthetics computed using model A8b2 show significantly better fits to observed data for the 1992 Yellow Sea earthquake than do synthetics computed with model A8.

A crucial point in this report is that the same crustal model is used for all stations and earthquakes. The rationale for this is threefold. First, the dominant frequency of the CDSN LH seismograms is near 40 sec, with a wavelength of 140-150 km. This wavelength effectively averages over small-scale variations in crustal structure. Second, inversions for the 3 November 1992 earthquake attained good agreement between synthetics and observed data with a single model, suggesting that in northeastern China the crust can indeed be approximated by a single layered model. Third, use of a single structural model reduces the number of free parameters in the inversion. The approach in

this report is to assume a single crustal model for the entire region, then invert for the earthquake source. The refined source parameters can then be used to further refine the structural model. In this way, the inversion for each set of parameters is isolated from the other. Note that the time-shift feature of the inversion algorithm provides a limited means of accounting for variations in crustal structure. The implications of the observed time shifts are discussed below.

Table 3. Crustal Model A8b2

Depth km	P-velocity km/s	Q_p	S-velocity km/s	Q_S	Density g/cm^3
0.0	5.06	50	2.93	25	2.33
1.0	5.06	50	2.93	25	2.33
1.0	5.42	100	3.13	50	2.58
3.0	5.42	100	3.13	50	2.58
3.0	6.16	525	3.56	263	2.75
16.0	6.16	525	3.56	263	2.75
16.0	6.80	525	3.92	263	2.83
35.0	6.80	525	3.92	263	2.83
35.0	8.04	525	4.47	263	3.23
120.0	8.05	525	4.50	263	3.30
210.0	8.30	525	4.52	263	3.40
410.0	9.03	525	4.87	263	3.67
410.0	9.36	525	5.07	263	3.80
660.0	10.20	525	5.60	263	4.12
660.0	10.79	525	5.95	263	4.34
760.0	11.06	525	6.21	263	4.44

4. FOCAL MECHANISM INVERSIONS

4.1 22 January 1992

This Ms 4.8 event occurred in the western Yellow Sea at the default PDE depth of 33 km. Two inversion runs were made for this earthquake: the first which used only the LH waveforms at four stations, and the second which used waveforms and the first-motion constraint with no incorrect polarities allowed (Table 4). Both inversions give nearly identical focal mechanisms with the inversion run using only the LH waveforms having a slightly, but not significantly, better L2 norm value than the case of waveforms plus polarities. The waveform plus polarity inversion result is shown in Figure 4.

Table 4. Inversion Results

Earthquake	Stations used	L2 Norm	Depth (km)	Strike (deg)	Dip (deg)	Rake (deg)
22 January 1992	BJI, HIA, LZH, MDJ					
LH waveforms only		0.61340	12	197	51	128
waveforms & f-m polarities (0 incorrect)		**0.64982**	**12**	**197**	**54**	**127**
3 November 1992	BJI, ENH, MDJ, HIA,SSE, LZH					
Nugyen (1994)		0.96321[1]	9	15	80	155
LH waveforms only w/A5 (Cipar, 1995)		1.00050	15	19	90	173
LH waveforms only w/A8b2		0.69277	15	17	89	170
waveforms & f-m polarities (1 incorrect)		**0.82777**	**15**	**18**	**84**	**166**
30 December 1993	ENH, HIA, LZH, MDJ					
LH waveforms only		**0.94557**	**15**	**29**	**90**	**177**
25 July 1994	HIA, LZH, MDJ, SSE, KMI (polarity only)					
LH waveforms only		0.82108	15	211	89	183
waveforms & f-m polarities (1 incorrect)		0.94037	12	211	84	180
waveforms & f-m polarities (0 incorrect)		**0.95097**	**12**	**210**	**82**	**179**
USGS centroid moment tensor solution		-	15	196	90	-180
11 August 1995	HIA, MDJ, SSE					
waveforms & f-m polarities		**0.37372**	**9**	**72**	**47**	**258**

[1] computed using grid search algorithm

4.2 3 November 1992

This earthquake has been studied by Nguyen and Hsu (1993) and Nguyen (1994) who determined its focal mechanism by inverting CDSN LH-band surface-wave seismograms. Cipar (1995) used the same data set to determine the depth and focal mechanism by the grid search algorithm, and a refinement to the regional Earth model by reflectivity modeling. Note that Cipar's (1995) inversion used LH surface-wave synthetics computed with the A5 model for Korea and northeastern China. The focal mechanisms determined by Nguyen (1994) and Cipar (1995) are given in Table 4 and shown in Figure 5, along with two mechanisms determined in this report. The inversions reported in this report use synthetics computed with the most recent crustal model, A8b2, both with and without the P-wave polarity test. While the four mechanisms are broadly similar to each other, the best surface wave mechanism and P-wave polarity mechanisms are inconsistent. The best-fitting surface-wave mechanism using the waveforms only with model A8b2 (Figure 5c) does not fit the clear positive first-motion at ENH. On the other hand, Nguyen's (1994) mechanism (Figure 5a), which fits the P-wave polarity readings, produces significantly degraded surface wave fits (Table 4). One explanation is that a small dilatational first motion at ENH is obscured by the ambient noise. The observed and synthetic waveforms for the preferred model (boldface type in Table 4) are shown in Figure 6.

4.3 30 December 1993

This earthquake in northeastern China is located approximately 200 km northwest of the North Korean event of 11 August 1995, and is a useful comparison to that event. Considerable noise on the broadband stations obscured first motion readings at the CDSN stations. The LH waveforms at four stations (Table 4) were used to invert for the mechanism. The best fit between observed and synthetics was found at a source depth of 15 km with the focal mechanism shown in Figure 7.

4.4 25 July 1994

This event occurred in the southern Yellow Sea, close to and somewhat larger than the 3 November 1992 earthquake. Because of its size, regional data exhibit excellent signal-to-noise ratio out to station KMI at a distance of 2353 km. Long-period (LH) seismograms from four CDSN stations and P-wave polarity readings from five were used in the inversion. Three inversion runs were made: the first relied solely on LH

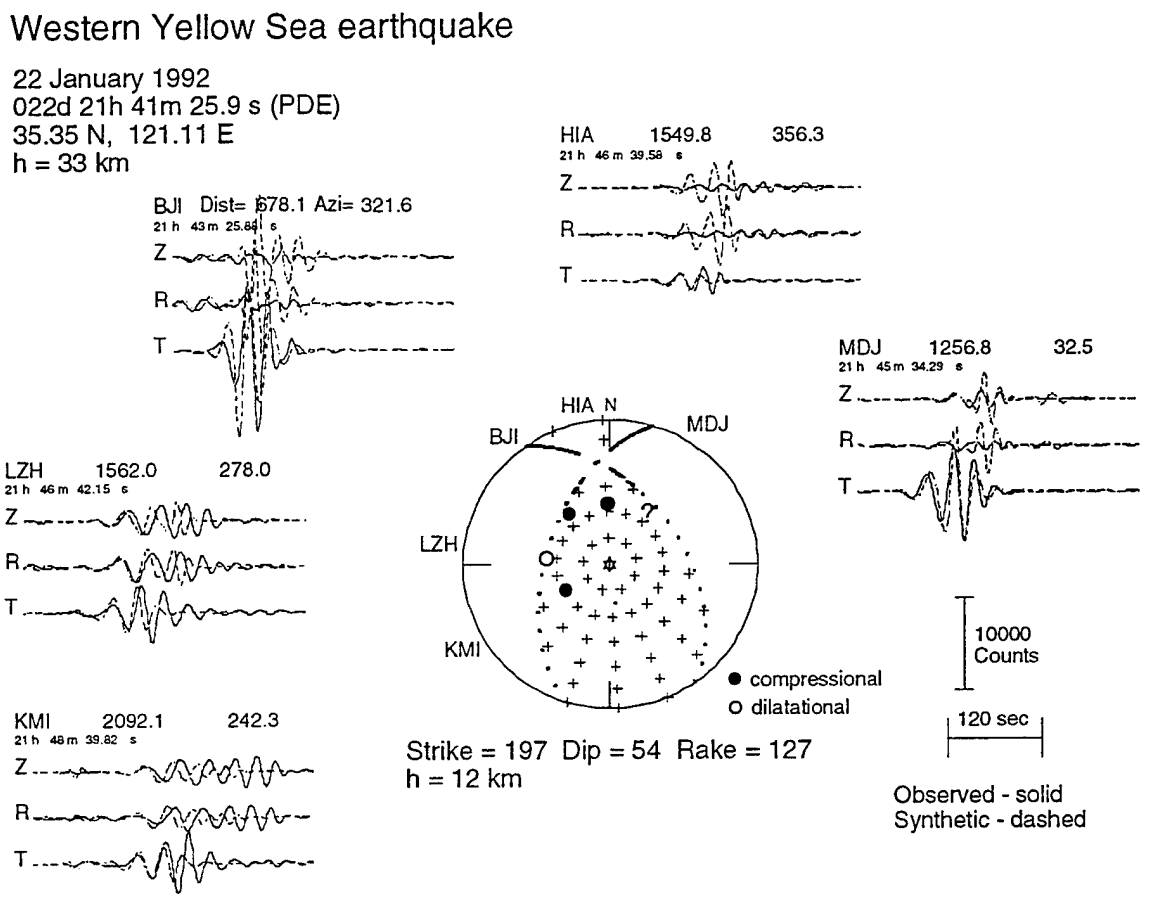

Figure 4. Observed (solid lines) and synthetic (dashed) LH seismograms for the western Yellow Sea earthquake of 22 January 1992 displayed as a function of azimuth around the P-wave focal mechanism. The station abbreviation (Table 2) is followed by the distance in kilometers and the azimuth in degrees. Note the time and amplitude scales. The mechanism shown corresponds to the preferred mechanism given in boldface type in Table 4. Compressional quadrants are indicated with plus signs; positive P-wave first motions are shown by filled dots, dilatational by open dots.

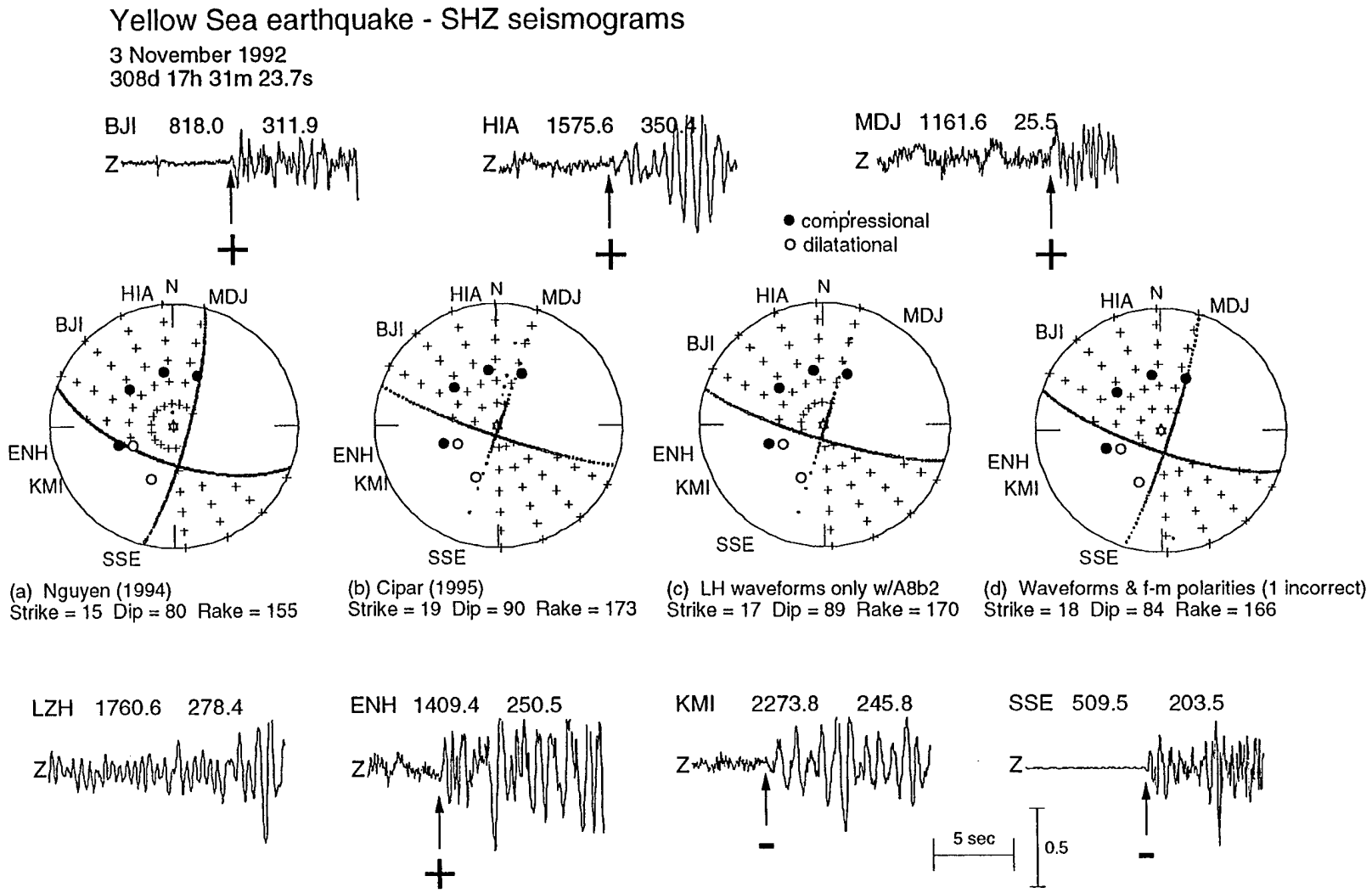

Figure 5. Short-period seismograms for the Yellow Sea earthquake of 3 November 1992, along with focal mechanisms determined using various data sets (see text and Table 4). Compressional quadrants are indicated with plus signs; positive P-wave first motions are shown by filled dots, dilatational by open dots.

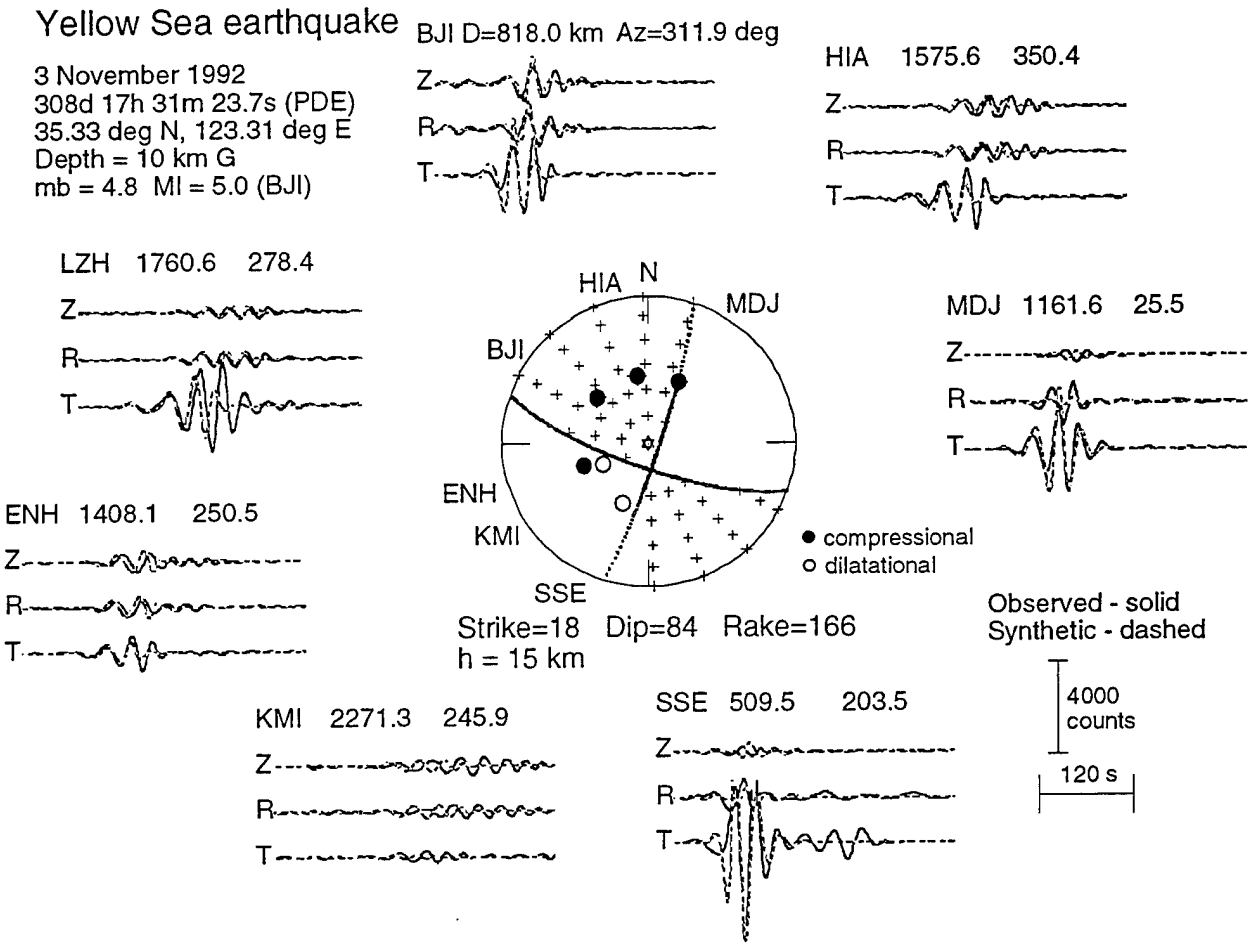

Figure 6. Observed (solid lines) and synthetic (dashed) LH seismograms for the Yellow Sea earthquake of 3 November 1992 displayed as a function of azimuth around the P-wave focal mechanism. The station abbreviation (Table 2) is followed by the distance in kilometers and the azimuth in degrees. Note the time and amplitude scales. The mechanism shown corresponds to the preferred mechanism given in boldface type in Table 4. Compressional quadrants are indicated with plus signs; positive P-wave first motions are shown by filled dots, dilatational by open dots.

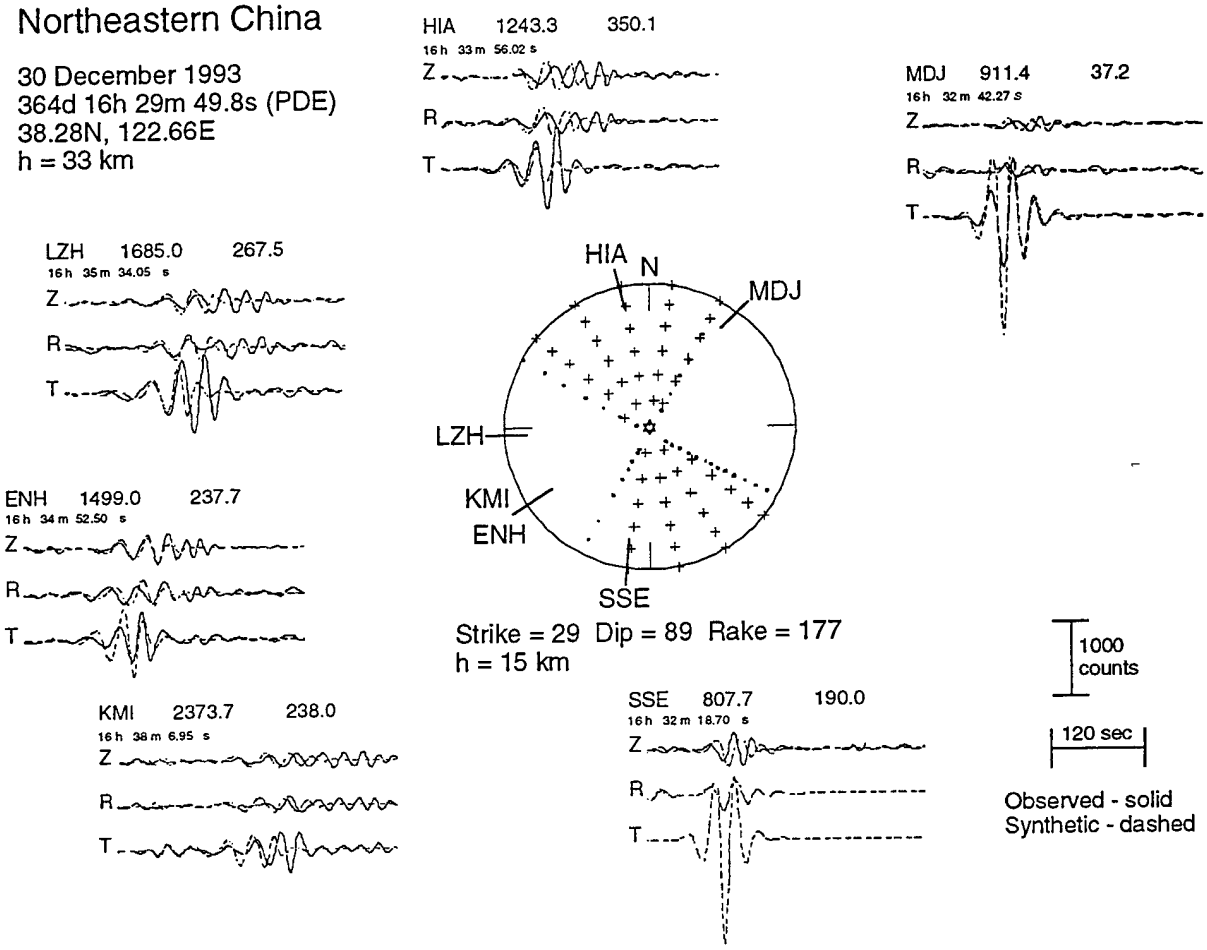

Figure 7. Observed (solid lines) and synthetic (dashed) LH seismograms for the Northeastern China earthquake of 30 December 1993 displayed as a function of azimuth around the P-wave focal mechanism. The station abbreviation (Table 2) is followed by the distance in kilometers and the azimuth in degrees. Note the time and amplitude scales. The mechanism shown corresponds to the preferred mechanism given in boldface type in Table 4. Compressional quadrants are indicated with plus signs; positive P-wave first motions are shown by filled dots, dilatational by open dots.

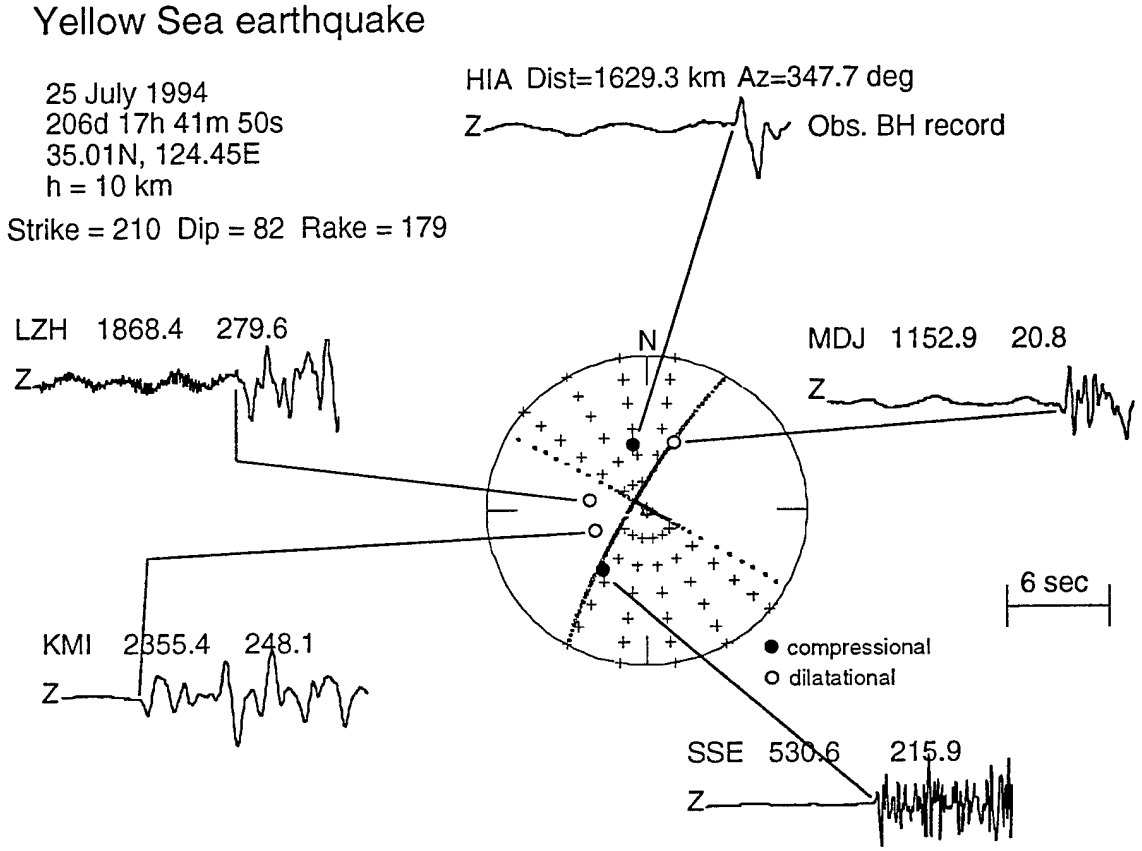

Figure 8. Broadband (BH) vertical seismograms for the 25 July 1994 Yellow Sea earthquake illustrating the first-motion observations. The mechanism shown corresponds to the preferred mechanism given in boldface type in Table 4. Compressional quadrants are indicated with plus signs; positive P-wave first motions are shown by filled dots, dilatational by open dots.

waveforms; the second used the waveforms and the first motion test allowing 1 incorrect P-wave polarity; and the third used the waveforms and first motions with 0 incorrect polarities (Table 4). Also given in Table 4 is the USGS centroid moment tensor (CMT) solution for this earthquake. Figure 8 shows the P-wave portion of the broadband (BH) records for five stations with clear first motions, along with the focal mechanism plot for the preferred solution using waveforms with 0 incorrect first-motion polarities (Table 4). Focal mechanisms for each solution given in Table 4 are shown in Figure 9. Note that the inversion mechanisms determined in this report (top row) are quite similar, with parameter changes of only a few degrees. The inversion using only the LH waveforms gives the best L2 norm misfit, but predicts 2 incorrect polarities (MDJ and SSE). The inversions for waveforms plus 1 or 0 incorrect polarities are quite similar and have almost the same L2 norm misfit values. The polarities at stations SSE and MDJ provide strong constraints on the NE-SW-striking nodal plane, which, in turn, controls the mechanism. Figure 10 compares the observed and synthetic LH seismograms computed for the preferred solution (bold type in Table 4). Agreement in both amplitude and phase is quite good at the nearer stations. Station KMI was not used in the inversion, however the combination of mechanism and structure do a good job of predicting the amplitudes, but do not do quite so well for the phase.

4.5 11 August 1995

This event in North Korea is the smallest of the five, but from the standpoint of CTBT monitoring the most important. Good records are available at four stations within 1300 km, including the IRIS station at Inchon, South Korea (INCN). Clear down first motion polarities were read at MDJ and INCN and incorporated as constraints on the waveform inversion. The best fitting focal mechanism is a nearly east-west striking normal fault at a depth of 9 km. Observed and synthetic LH waveforms for this mechanism are shown in Figure 11. There is no independent determination of the focal mechanism or depth for this event.

5. DISCUSSION

5.1 Focal Mechanisms and Depths

With the exception of the 25 July 1994 event, the small size of the earthquakes discussed in this report precluded independent teleseismic determination of the focal mechanism and depth. The USGS CMT solution for the 25 July 1994 earthquake is broadly consistent with the mechanism determined in this report in that both are left-

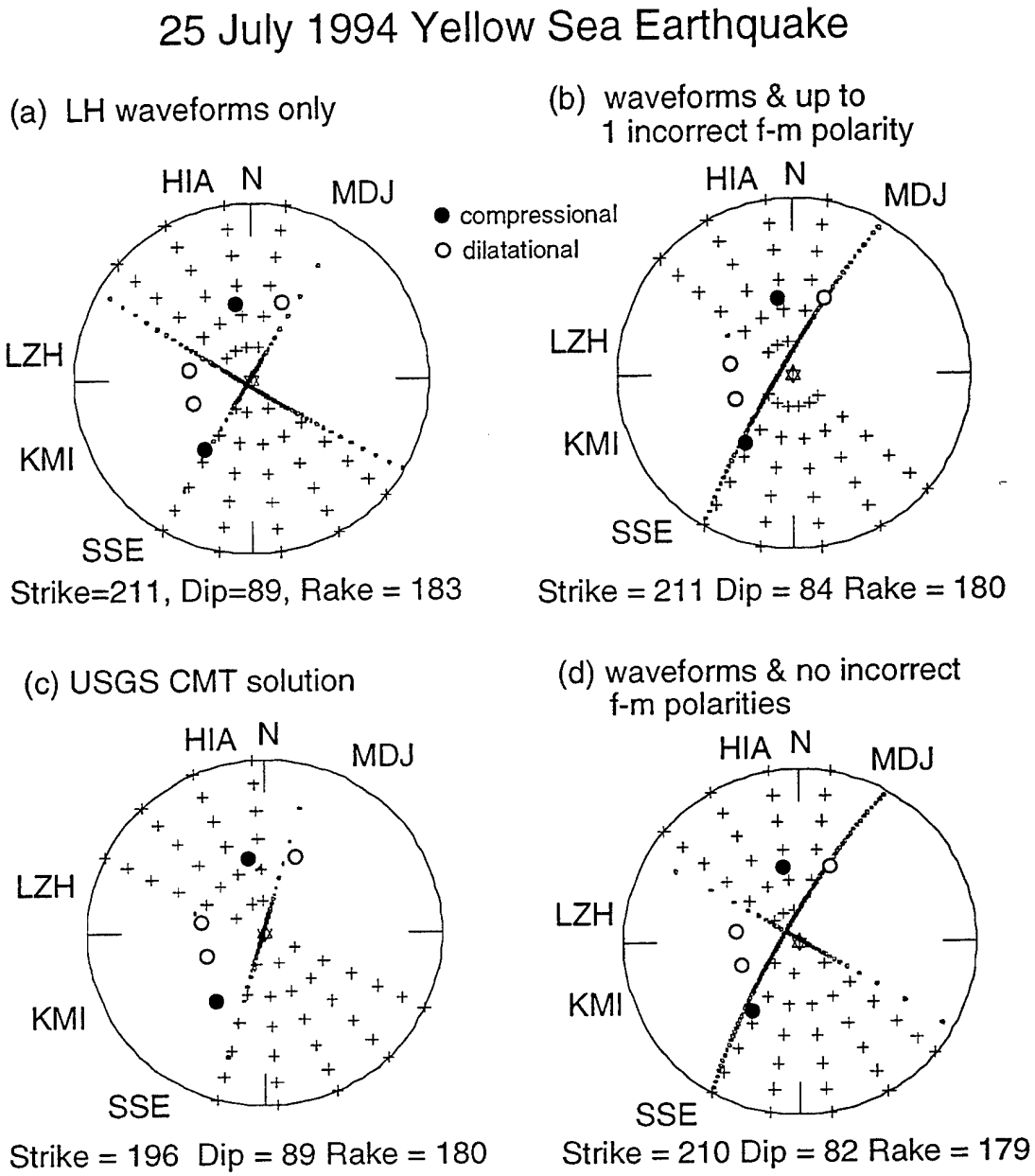

Figure 9. Comparison of focal mechanisms determined by various methods for the Yellow Sea earthquake of 25 July 1994. See Table 4 and discussion in text. Compressional quadrants are indicated with plus signs; positive P-wave first motions are shown by filled dots, dilatational by open dots.

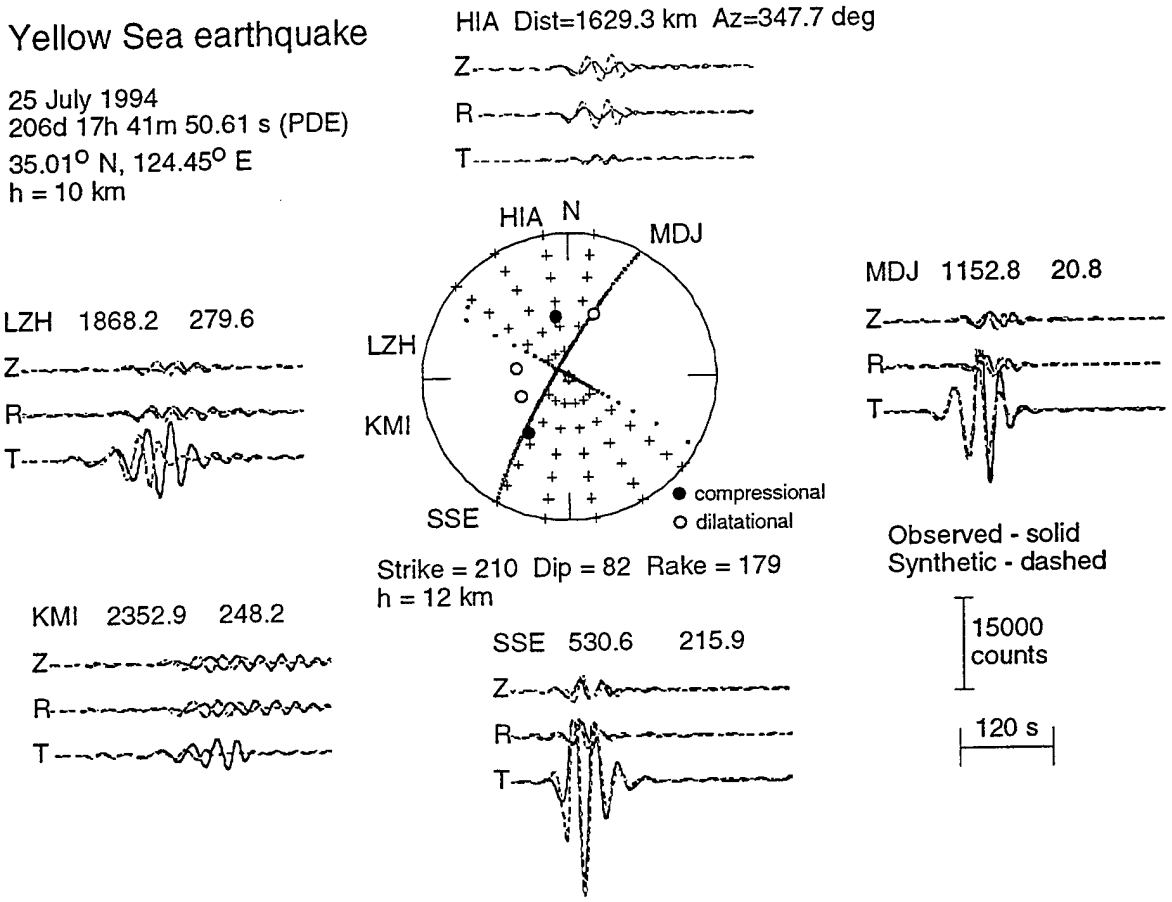

Figure 10. Observed (solid lines) and synthetic (dashed) long-period (LH) seismograms for the Yellow Sea earthquake of 25 July 1994 displayed as a function of azimuth around the P-wave focal mechanism. The station abbreviation (Table 2) is followed by the distance in kilometers and the azimuth in degrees. Note the time and amplitude scales. The mechanism shown corresponds to the preferred mechanism given in boldface type in Table 4. Compressional quadrants are indicated with plus signs; positive P-wave first motions are shown by filled dots, dilatational by open dots.

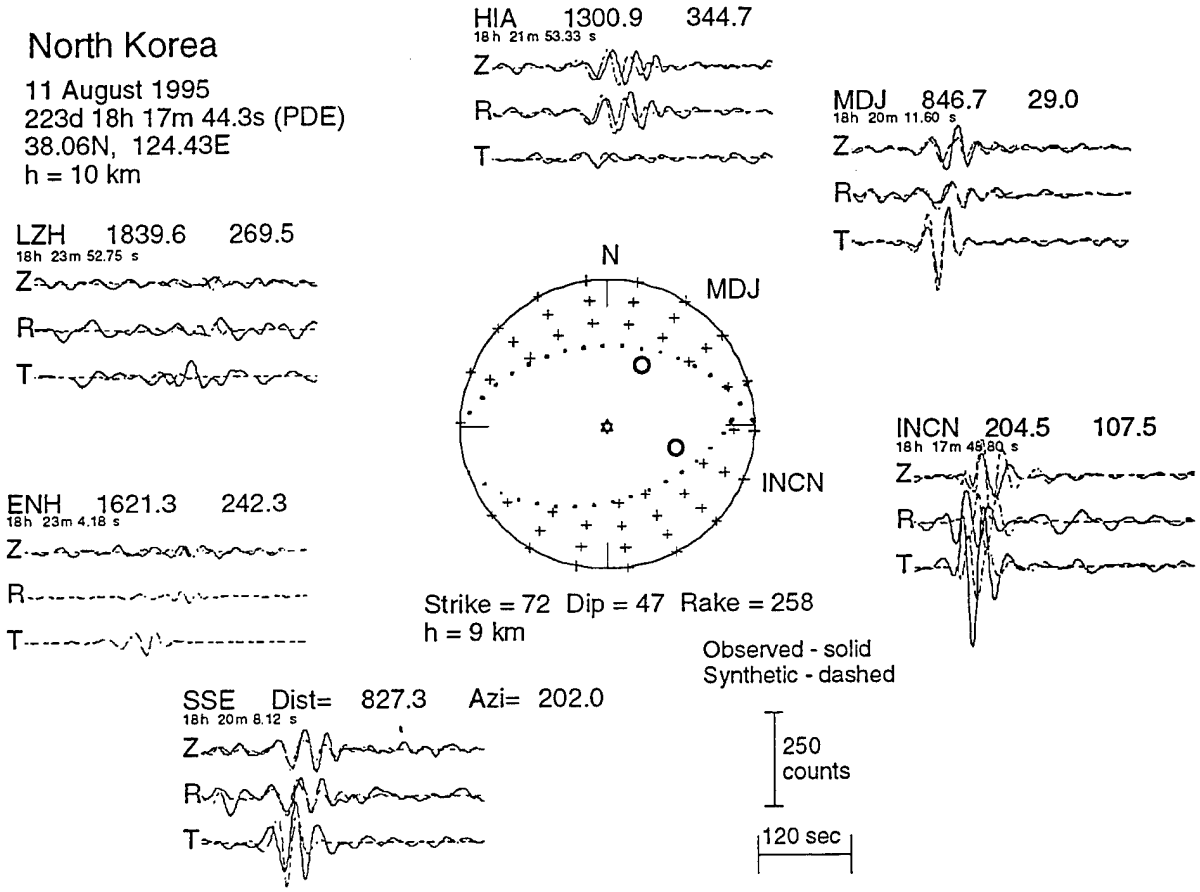

Figure 11. Observed (solid lines) and synthetic (dashed) long-period (LH) seismograms for the North Korea earthquake of 11 August 1995 displayed as a function of azimuth around the P-wave focal mechanism. The station abbreviation (Table 2) is followed by the distance in kilometers and the azimuth in degrees. Note the time and amplitude scales. The mechanism shown corresponds to the preferred mechanism given in boldface type in Table 4. Compressional quadrants are indicated with plus signs; positive P-wave first motions are shown by filled dots, dilatational by open dots.

lateral strike-slip (Figure 9). Similar left-lateral strike-slip mechanisms along west-northwest trending faults have been determined for several large events in this region using teleseismic observations (Cipar, 1979; Chung and Cipar, 1983; Chung and Brantley 1989). These are in good agreement with the preferred mechanisms for the earthquakes of 3 November 1992, 30 December 1993, and 25 July 1994 (Figure 12). The North Korean (11 August 1995) and western Yellow Sea (22 January 1992) earthquakes, on the other hand, have quite different mechanisms. These earthquakes may be the result of minor thrust faulting accompanying the overall strike-slip stress regime. Likewise the depths determined for the large events are shallow, generally <10 km, in good agreement with the focal depths determined in this study.

5.2 Observed Time Delays

As discussed above, the inversion algorithm has a feature that allows the synthetic to be shifted in time relative to the observed record. This time shift is a variable in the inversion, and in general leads to improved synthetic-observed fits. In this report, the maximum allowed time shifts were +/- 10 seconds. The time delays corresponding to the preferred focal mechanisms (bold face type in Table 4) are given in Table 5 by station and event. A negative time shift means that the data are slow with respect to the synthetic. These time shifts can be ascribed either to uncertainty in the origin time and/or overall crustal velocity (common to all stations), or to uncertainty in event location and/or differences in group velocity along each travel path (station specific). The event averages (bottom row in Table 5) appear to correlate inversely with event size, in that the smaller events have delays of -2 to -3 s, while the large events have <1 sec delays. This effect can be ascribed to clearer P-wave observations for the larger events that lead to more accurate locations and origin times.

The average delay for each station is given in the last column. An incorrect event location of 10 km can contribute ~2.5 s to individual station delays for each event. On the other hand, the -5.6-s delay at HIA can be explained by a 1 to 2 percent change in velocity over the average source-to-station travel path of 1500 km. The observed delays probably are composed of both effects, and it is premature to infer crustal velocity variations using these observations. Nevertheless, the observation of -1 to -2-s delays at most stations is a strong argument for the use of a single crustal model for northeastern China.

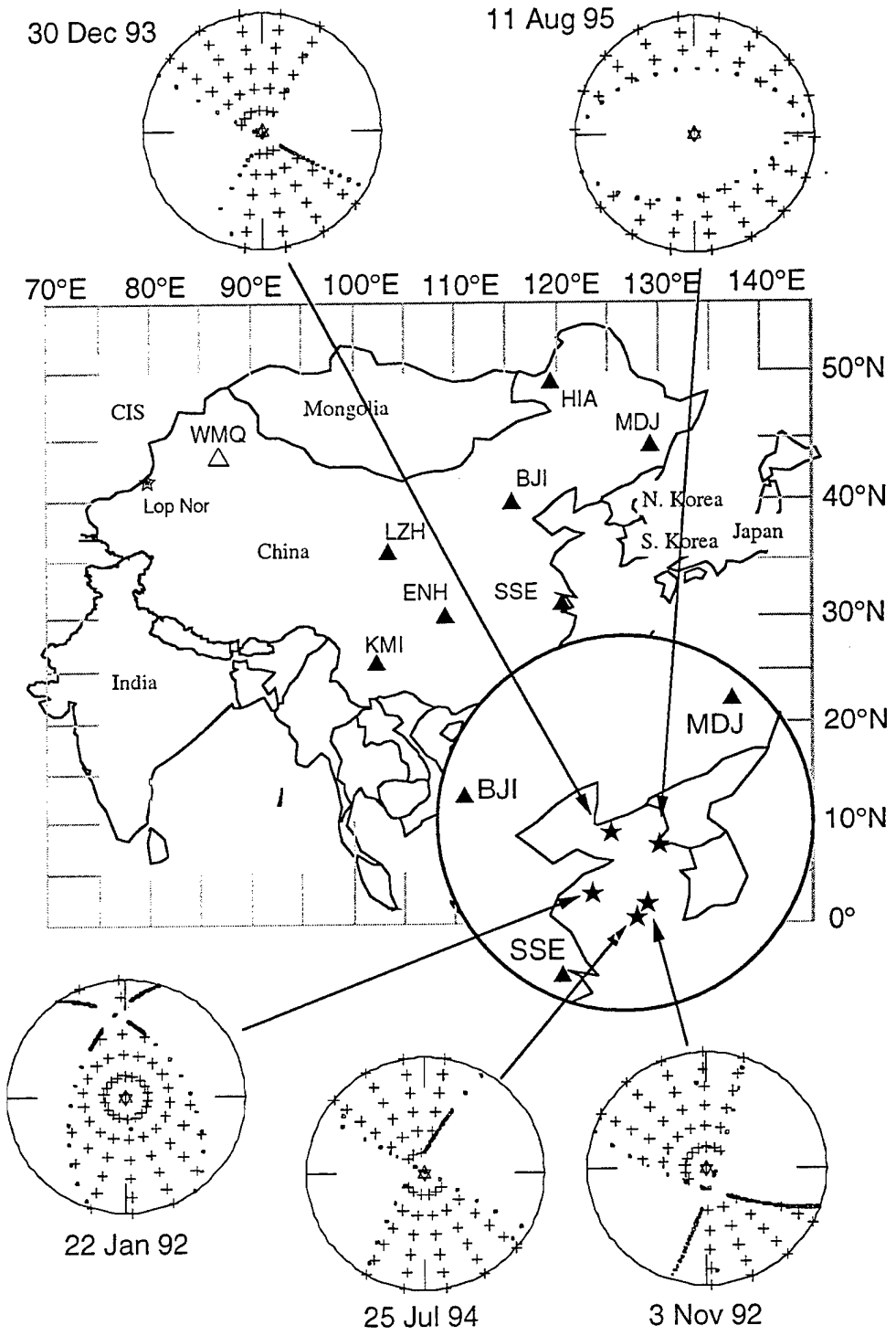

Figure 12. Map of eastern Asia showing a compilation of focal mechanisms determined in this report. Compressional quadrants are indicated with plus signs; positive P-wave first motions are shown by filled dots, dilatational by open dots.

Table 5. Observed Time Delays

Station	22 Jan 92	3 Nov 92	30 Dec 93	25 Jul 94	11 Aug 95	Station Average
BJI	+4.0	+1.0				+2.5
HIA	-5.0	-3.0	-10.0	-4.0	-6.0	-5.6
LZH	-9.0	-1.0	-5.0	+6.0		-2.25
MDJ	1.0	1.0	-2.0	-3.0	-1.0	-0.8
SSE		3.0		+1.0	+2.0	2.0
ENH		-5.0	4.0			-0.5
Event Average	-2.25	-0.67	-3.25	+0.0	-1.7	

6. CONCLUSIONS

The grid search algorithm for determining earthquake focal mechanism and depth is tested by inverting regional-distance seismograms for a suite of five earthquakes in northeastern China and Korea. An improved crustal model for the region is used to compute the synthetic Green's functions for the fundamental fault types. The algorithm combines these to form realistic synthetics, which are compared directly to the observed data using an L2 norm test. To account for uncertainty in timing, location, and crustal structure, the synthetics are time-shifted during the inversion to produce the best match. This process is repeated for a range of source depths. An improvement to the algorithm reported in this report is the use of P-wave polarity readings as a further constraint on the allowed mechanism. The focal mechanisms and depths for the earthquakes studied in this report are broadly consistent with teleseismic measurement of earlier large events in the region. The average time delays at each station and for each event provide a measure of the uncertainty in origin time and velocity structure. Crustal velocity variations of 1 to 2 percent could explain the observed delays, supporting the assumption of a single crustal model for northeastern China. On the other hand, the delays at most stations can be accounted for by incorrect event locations of ~10 km.

References

Chung, Wai-Ying and Benjamin J. Brantley (1989). The 1984 Southern Yellow Sea Earthquake of Eastern China: Source Properties and Seismotectonic Implications for a Stable Continental Area, *Bull. Seism. Soc. Am.,* **79**, 1863-1882.

Chung, Wai-Ying and John J. Cipar (1983). Source Modeling of the Hsingtai, China, Earthquakes of March, 1966, *Phys. of Earth and Planet. Int.*, **13**, 85-96.

Cipar, John J. (1979). Source Processes of the Haicheng, China, Earthquake from Observations of P- and S-waves, *Bull. Seism. Soc. Am.,* **69**, 1903-1916.

Cipar, J. (1995). A Grid Search Algorithm to Determine Earthquake Source Parameters - Application to the 1992 Yellow Sea, China, Earthquake, PL-TR-95-2082, Env. Res. Paper 1171, 8 June 1995, ADA302221

Fuchs, K. and G. Muller (1971). Computation of Synthetic Seismograms with the Reflectivity Method and Comparison with Observations, *Geophys. J. Roy. Astron. Soc.,* **23,** 417-433.

Kennett, B. L. N. (Editor) (1991). *IASPEI 1991 Seismological Tables,* Australian National University, 167p.

Menke, William (1984). *Geophysical Data Analysis: Discrete Inverse Theory,* Academic Press, 1984, 260p.

Muller, G. (1985). The Reflectivity Method: A Tutorial, *Jour. of Geophys.,* **58,** 153-174.

Nguyen, Bao V. (1994). Surface-Wave Focal Mechanism of the 03 November 1992 Yellow-Sea Main Shock, *EoS (Trans. Am. Geophys. Union),* **75,** 241.

Nguyen, Bao V. and Vindell Hsu (1993). Shear Path Structures from Inversions of Surface Waves of the 03 November 1992 Yellow-Sea Main Shock, *EoS (Trans. Am. Geophys. Union),* **74,** 426.

Zhao, Lian-She and Donald V. Helmberger (1994). Source Estimation from Broadband Regional Seismograms, *Bull. Seism. Soc. Am.,* **84,** 91-104.